

## Locating an atmospheric contamination source using slow manifolds

Wenbo Tang,<sup>1</sup> George Haller,<sup>2,a)</sup> Jong-Jin Baik,<sup>3</sup> and Young-Hee Ryu<sup>3</sup>

<sup>1</sup>*School of Mathematical and Statistical Sciences, Arizona State University, Tempe, Arizona 85287, USA*

<sup>2</sup>*Department of Mechanical Engineering, Massachusetts Institute of Technology, Cambridge, Massachusetts 02139, USA*

<sup>3</sup>*School of Earth and Environmental Sciences, Seoul National University, Seoul 151-742, South Korea*

(Received 30 May 2008; accepted 11 March 2009; published online 14 April 2009)

Finite-size particle motion in fluids obeys the Maxey–Riley equations, which become singular in the limit of infinitesimally small particle size. Because of this singularity, finding the source of a dispersed set of small particles is a numerically ill-posed problem that leads to exponential blowup. Here we use recent results on the existence of a slow manifold in the Maxey–Riley equations to overcome this difficulty in source inversion. Specifically, we locate the source of particles by projecting their dispersed positions on a time-varying slow manifold, and by advecting them on the manifold in backward time. We use this technique to locate the source of a hypothetical anthrax release in an unsteady three-dimensional atmospheric wind field in an urban street canyon. © 2009 American Institute of Physics. [DOI: 10.1063/1.3115065]

### I. INTRODUCTION

Small inertial particles in a fluid flow and ideal fluid tracers behave differently, even if they have the same density. This is because ideal tracers follow the infinitesimal fluid particle motion generated by the fluid velocity field, while inertial particle dynamics is governed by the Maxey–Riley equations (cf. Maxey and Riley).<sup>1</sup> These equations describe the motion of a small rigid sphere in an unsteady Stokes flow. Auton *et al.*<sup>2</sup> derived a correction to the added mass term in the equations. This correction, however, is insignificant for small particles, and hence will be neglected in this paper.

Because of the wide range of their applications, the Maxey–Riley equations have been studied extensively in all regimes where the particle density is larger (aerosol), equal to (neutrally buoyant) or less (bubble) than the fluid density.<sup>3–6</sup> As mentioned in Benczik *et al.*,<sup>4</sup> an important application of such studies is pollutant-transport forecasting for homeland defense and threat reduction purposes. Equally important is locating the source of a toxin or biological pathogen spill from outbreaks based on sensor data and available large-scale flow information.

The Maxey–Riley equations, in principle, give a tool for locating the origin of atmospheric particle pollution from dispersed particle positions, provided that diffusion effects are negligible. In practice, such a source inversion procedure is challenging due to a strong instability of the equations in backward time. Because of this instability, even high-precision numerical schemes lead to a blowup of backward-time trajectories, and hence source identification cannot be achieved in a reasonable time with reasonable accuracy.

Recently, Haller and Sapsis<sup>7</sup> overcame this instability problem by inverting the flow of particles on a lower-dimensional slow manifold, which they constructed explicitly for any type of finite-size particle (bubble, aerosol, or suspension). This source inversion procedure renders the initial location of particle release, but not the initial velocity of the particles; the latter information is lost due to the reduction to the slow manifold. The initial position, however, is located with high accuracy and little computational effort, because the strong instability mentioned above lies in a direction transverse to the slow manifold.

In the present paper, we implement the above source inversion approach for the first time in a spatially complex three-dimensional unsteady flow. Motivated by homeland security applications, we consider a hypothetical anthrax release event in a three-dimensional unsteady wind field inside an urban street canyon. The numerical data of the urban flow was generated from an unsteady Reynolds-averaged Navier–Stokes (RANS) equation model using the renormalization group  $k-\varepsilon$  turbulence closure. Unsteady RANS approaches are described in many papers (e.g., Sini *et al.*<sup>8</sup>); the flow geometry is set to be the same as Kim and Baik,<sup>9</sup> unsteadiness is introduced via varying ambient wind speed.

In this urban flow, we compute both the slow manifold and the inertial equation that governs the dynamics on the slow manifold. We first demonstrate that source inversion fails when high-precision numerical integration is attempted on the solutions of the full six-dimensional Maxey–Riley equations. We then show how source inversion can be carried out using the inertial equation on the three-dimensional slow manifold.

Although demonstrated here only for an urban flow example, source inversion in other turbulent flows can be carried out in the same manner, provided that the Maxey–Riley equations are valid for the particles considered.

<sup>a)</sup>Author to whom correspondence should be addressed. Electronic mail: ghaller@mit.edu.

## II. GOVERNING EQUATIONS

Following several prior studies,<sup>5,7,10</sup> we neglect the effects of the Basset history force in the original Maxey–Riley equations. Due to the small size we assume for the particles, the Faxén correction term is also negligible (cf. Benczik *et al.*).<sup>4</sup> Under these assumptions the nondimensionalized particle position  $\mathbf{x}(t)$  and particle velocity  $\mathbf{v}(t)$  at time  $t$  satisfy the simplified Maxey–Riley equations

$$\dot{\mathbf{x}} = \mathbf{v}, \quad \dot{\mathbf{v}} - \frac{3R}{2} \frac{D\mathbf{u}}{Dt} = -\frac{1}{\epsilon}(\mathbf{v} - \mathbf{u}) + \left(1 - \frac{3R}{2}\right)\mathbf{g}, \quad (1)$$

where  $\mathbf{g}$  is the vector of gravity,  $\mathbf{u}$  is the ambient fluid velocity, and

$$R \equiv \frac{2\rho_f}{\rho_f + 2\rho_p}, \quad St \equiv \frac{2}{9} \left(\frac{a}{L}\right)^2 Re_f, \quad \epsilon \equiv \frac{St}{R}.$$

Here  $\rho_f$  and  $\rho_p$  are the densities of the fluid and of the particle, respectively;  $R$  is the density ratio distinguishing neutrally buoyant particles ( $R=2/3$ ) from aerosols ( $0 < R < 2/3$ ) and bubbles ( $2/3 < R < 2$ );  $a$  is the radius of the spherical particle;  $L$  is a characteristic length scale of the flow; the fluid Reynolds number is  $Re_f \equiv UL/\nu$ , with typical large-scale fluid velocity  $U$  and fluid viscosity  $\nu$ ; time is nondimensionalized with the characteristic time scale  $L/U$ .

The Stokes number  $St$  measures the dimensionless response time of the particle motion due to the characteristic ambient time scale  $L/U$ ;<sup>14</sup>  $\epsilon$  quantifies the importance of inertia. The limit  $\epsilon \rightarrow 0$  corresponds to ideal passive tracers; the effect of inertia is more pronounced with larger  $\epsilon$ . For the Maxey–Riley equations and Eq. (1) to be a valid approximation, the particle motion must satisfy  $a/L \ll 1$ ,  $Re_p \equiv (|\mathbf{v} - \mathbf{u}|)a/\nu \ll 1$  and  $St \ll 1$ , where  $Re_p$  is the particle Reynolds number.

## III. SLOW MANIFOLD AND INERTIAL EQUATION

There have been several studies discussing the asymptotics of Maxey–Riley equations for *steady* flows.<sup>10–12</sup> More recently, Haller and Sapsis<sup>7</sup> derived general results for the equations under unsteady flow conditions, which are the focus of the present paper.

Since  $St \ll 1$ ,  $\epsilon$  is a small number, we can introduce the fast time  $\tau$  via  $dt/d\tau = \epsilon$ . Haller and Sapsis<sup>7</sup> prove that a globally attracting three-dimensional, time-dependent invariant manifold  $M_\epsilon$  exists in the six-dimensional phase space of Eq. (1).  $M_\epsilon$  is a slow manifold that can be written in the form

$$M_\epsilon = \left\{ (\mathbf{x}, \mathbf{v}) : \mathbf{v} = \mathbf{u} + \epsilon \left( \frac{3R}{2} - 1 \right) \left[ \frac{D\mathbf{u}}{Dt} - \mathbf{g} \right] + \mathcal{O}(\epsilon^2) \right\}. \quad (2)$$

Particle motion on the slow manifold satisfies the *inertial equation*<sup>7</sup>

$$\dot{\mathbf{x}} = \mathbf{u}(\mathbf{x}, t) + \epsilon \left( \frac{3R}{2} - 1 \right) \left[ \frac{D\mathbf{u}(\mathbf{x}, t)}{Dt} - \mathbf{g} \right] + \mathcal{O}(\epsilon^2). \quad (3)$$

Analogous equations were also derived by Refs. 5 and 13–16

using formal asymptotic expansions of the velocity field. The invariant manifold approach used by Haller and Sapsis<sup>7</sup> justifies these formal solutions. The approach also yields a spatially dependent bound on  $\epsilon$  over which Eq. (3) loses its relevance due to the instability of the slow manifold (Sapsis and Haller<sup>17</sup>). The stability bound derived there is for neutrally buoyant particles, but we can obtain such a bound for aerosols in the same fashion.

The truncated first-order approximation to the particle velocity for arbitrary density can be written as

$$\frac{d}{dt}(\mathbf{v} - \mathbf{u}) = -(\mathbf{v} - \mathbf{u}) \left( \frac{3R}{2} \nabla \mathbf{u} + \frac{1}{\epsilon} \mathbf{I} \right) + \left( 1 - \frac{3R}{2} \right) \mathbf{g}, \quad (4)$$

where  $\mathbf{I}$  is the identity matrix. For small and heavy particles ( $R \ll 1$ ), the last term on the right-hand side of Eq. (4) is negligible. We, however, keep the  $(3R/2)\nabla \mathbf{u}$  term since the flow gradients can be large.

Using the results of Sapsis and Haller,<sup>17</sup> we find that for the slow manifold to remain as an attractor for inertial particle velocity, we must have

$$\lambda_{\min} \left[ \mathbf{I} + \frac{3\epsilon R}{2} \mathbf{S}(\mathbf{x}, t) \right] > 0. \quad (5)$$

Here  $\lambda_{\min}[\mathbf{I} + (3\epsilon R/2)\mathbf{S}]$  is the minimum eigenvalue of the matrix  $\mathbf{I} + (3\epsilon R/2)\mathbf{S}$ , with  $\mathbf{S} = [\nabla \mathbf{u} + (\nabla \mathbf{u})^T]/2$  denoting the rate-of-strain tensor. Over any fixed spatial and temporal domain of interest, condition (5) specifies an upper bound on  $\epsilon$  below which the inversion procedure described in the following section is valid.

## IV. SOURCE INVERSION USING THE SLOW MANIFOLD

For any initial position and for small enough  $\epsilon$ , particle motions will converge to the slow manifold  $M_\epsilon$  and synchronize with solutions of Eq. (3). In forward time, therefore, the asymptotic dynamics of the full Maxey–Riley Eqs. (1) are captured by the inertial Eq. (3).

Now consider the problem of locating the source of some nondiffusive contamination by finite-size particles. This problem involves solving Eq. (1) in backward time from known dispersed positions until the trajectories all reach a small enough volume considered the source. In principle, Eq. (1) has unique regular solutions in backward time, but the  $-\mathbf{v}/\epsilon$  term causes an inevitable blowup of numerical solutions over longer time scales. Reducing the integration time step delays the blowup process, but also significantly increases the total time to locate the source.

Using the slow manifold  $M_\epsilon$ , the initial positions of dispersed particles can be recovered with an error of  $\mathcal{O}(\epsilon)$ .<sup>7</sup> The source inversion procedure leading to this result involves two steps: (i) projection onto the slow manifold by setting  $\mathbf{v}$  to be the right-hand side of Eq. (3) for the dispersed particles and (ii) solution of Eq. (3) starting from the projected dispersed positions. Note that Eq. (3) shows no instability in backward time, and hence its backward-time solutions are obtained without any numerical difficulty. If the trajectories obtained in this fashion approach each other within an  $\mathcal{O}(\epsilon)$  distance, then they are also  $\mathcal{O}(\epsilon)$  close to their source.<sup>7</sup>

## V. DATA SET

In this paper, we demonstrate the use of the above source inversion principle for a hypothetical anthrax release event in a three-dimensional unsteady wind field inside an urban street canyon. The geometry of the urban flow is an array of  $4 \times 4$  square buildings, the numerical data is generated from an unsteady RANS equation model using the renormalization group  $k-\epsilon$  turbulence closure.<sup>9</sup> The governing equations are solved on staggered grids using a finite volume method; improved resolution is placed near the ground and building walls. We focus our analysis on the center of this geometry since the flow is better resolved there.

The flow inside the urban canopy is induced by external flow upstream, blowing at an angle toward the positive  $x$ -direction. For the present analysis, unsteady ambient wind forcing with variable speed has been implemented to model gusty winds in the urban street canyon. The angle of attack, defined as the angle between the direction of the ambient wind and a unit vector in the positive  $x$  direction, is  $15^\circ$ . The time step in the numerical model is 0.05 s; we use model output at every 0.2 s to study the dynamics of finite-size particles in this flow. Following Kim and Baik,<sup>9</sup> we refer to the  $x$ -direction as West-East and  $y$ -direction as South-North.

The major flow structure inside the street canyon is a portal vortex originating from the Southeast corner of the upwind building, which reattach to the ground at different locations near the Northern corners of the buildings, depending on the ambient wind speed. With the incoming wind blowing at an angle, there is also a horseshoe vortex near ground at the Southwest corner of the downwind building. This vortex allows entrainment of fluid particles originated from the Southern streamwise canyon to traverse the spanwise canyon and exit to a Northern streamwise canyon. Our flow system introduces time dependence in a quasisteady fashion using unsteady RANS; the main flow features are the same as those discussed in detail in Kim and Baik.<sup>9</sup>

## VI. LAGRANGIAN COHERENT STRUCTURES IN THE FLOW

We visualize the flow structure inside the urban street canyon using direct Lyapunov exponents (DLE).<sup>18–20</sup> Specifically, we integrate the ordinary differential equation  $\dot{\mathbf{x}} = \mathbf{u}(\mathbf{x}, t)$  starting from position  $\mathbf{x}_0$  at time  $t_0$ , to obtain fluid particle trajectories  $\mathbf{x}(t; \mathbf{x}_0, t_0)$ . We then compute the largest eigenvalue  $\lambda_{\max}(t; \mathbf{x}_0, t_0)$  of the Cauchy–Green strain tensor  $[\partial \mathbf{x}(t; \mathbf{x}_0, t_0) / \partial \mathbf{x}_0]^T [\partial \mathbf{x}(t; \mathbf{x}_0, t_0) / \partial \mathbf{x}_0]$ , where  $A^T$  denotes the transpose of  $A$ . The DLE field over the set of initial positions  $\mathbf{x}_0$  is defined as  $\sigma_t^L(\mathbf{x}_0) = \ln[\lambda_{\max}(t; \mathbf{x}_0, t_0)] / [2(t - t_0)]$ . This quantity measures the largest rate of expansion among infinitesimal vectors originating from  $\mathbf{x}_0$ .

Local maximizing sets (ridges) of the DLE field are distinguished sets of fluid particles that repel nearby trajectories over the time of integration. We refer to such distinguished sets as *repelling Lagrangian coherent structures (LCSs)*, as they turn out to evolve as near-material surfaces.<sup>20,21</sup> Repelling LCS separate regions of different flow behaviors, and highlight the flow structures inside the street canyon in a frame-independent fashion.

When computed in backward time, ridges of the DLE field mark the position of attracting material surfaces, or *attracting LCS*. These distinguished material surfaces serve as local targets for particles, and hence their shape determines the main geometry of dispersed particle positions over longer time scales. Indeed, repelling and attracting LCS are finite-time analogs of stable and unstable manifolds.

In Fig. 1, we show the isosurface of 83% of the maximum of the backward-time DLE field. This isosurface approximates the strongest attracting LCS, providing the Lagrangian signature of a portal vortex as discussed in Kim and Baik.<sup>9</sup> As seen for this particular time, one of the footprints of the portal vortex is inside the spanwise canyon, whereas the other is at the Northeast edge of the upwind building.

To illustrate fluid motion near this canyon, we plot two infinitesimal fluid particle trajectories starting from the South of the upwind building. The fluid particle starting near the ground is entrained into the portal vortex. This particle motion highlights the swirling region, whereas the fluid particle starting above the buildings is advected by the flow outside the urban canopy, moving at almost  $15^\circ$  toward the positive  $x$ -direction at all times. The shape and location of the portal vortex varies with changes in the external forcing. For example, the footprint of the vortex at the Northeast edge of the upwind building moves to the Northwest edge of the downwind building at a later time of the simulation. Nevertheless, the portal vortex structure is prevalent over the duration of the simulation. Note that in Fig. 1, as in the rest of the paper, the plots are in dimensional units.

## VII. LOCATING THE SOURCE OF ANTHRAX RELEASE

We release a set of inertial particles representing anthrax spores inside the streamwise canyon to study the dispersion and source inversion of a hypothetical pollutant outbreak event. By a rough estimate, a typical anthrax spore of radius  $10 \mu\text{m}$  weighs about 500 times than an air blob of the same size.<sup>4</sup> The characteristic length scale of the model flow  $L = 9.56 \text{ m}$  is the width of the street canyon (same as the building width), and the characteristic velocity scale  $U = 3.5 \text{ m/s}$  is the time-averaged velocity norm at the upper boundary of the computational domain.

In this setting, we have the density ratio  $R \approx 2 \times 10^{-3}$ , aspect ratio  $a/L \approx 1.05 \times 10^{-6}$ , Stokes number  $St \approx 8.14 \times 10^{-7}$ , fluid Reynolds number  $Re_f = 3.35 \times 10^6$ . All this gives  $\epsilon \approx 4.07 \times 10^{-4}$ . Because finite-size particles converge to the slow manifold  $M_\epsilon$ , we compare the slow manifold velocity with the background velocity, finding that  $|\mathbf{v} - \mathbf{u}| \ll 1 \text{ m/s}$ , and hence the particle Reynolds number satisfies  $Re_p \ll 1$ . Additionally, the time scale over which molecular diffusion will carry anthrax spores across the building width is much greater than the advection time scale  $T = 2.73 \text{ s}$ . Therefore, we are within the regime of the validity of Eqs. (1)–(3).

We recall that the slow manifold  $M_\epsilon$  is a time-varying three-dimensional graph over the three-dimensional phase space of  $\mathbf{x}$  (or, equivalently, a time-independent four-dimensional graph over the extended phase space of the  $\mathbf{x}$

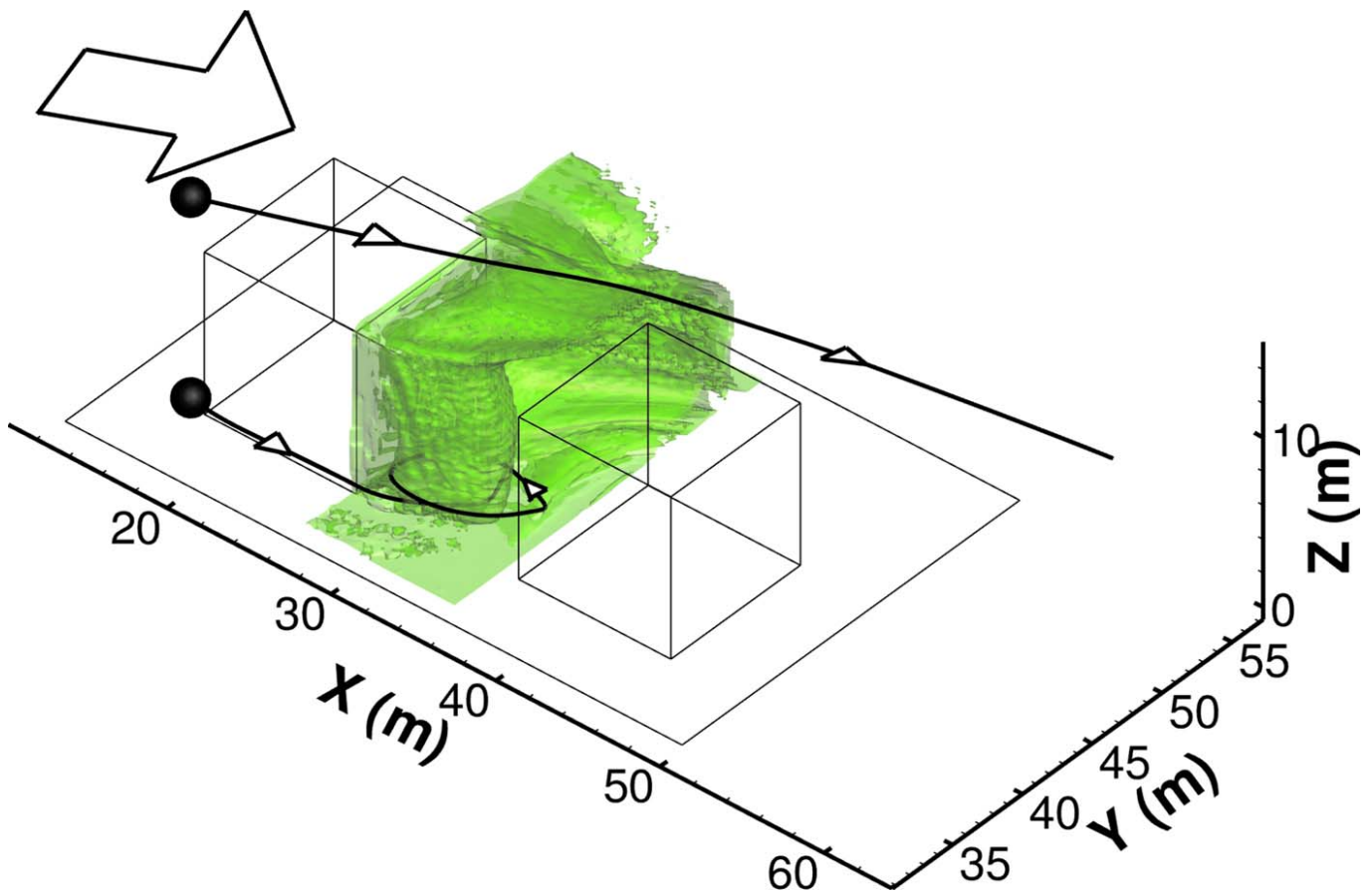


FIG. 1. (Color online) The view of an isosurface of the backward-time DLE field in the street canyon. The straight solid lines show the urban canyon geometry and the green isosurfaces outline the core of a portal vortex. The two black solid lines outline two *fluid particle* trajectories starting from the South of an upwind building, their directions marked by the small white triangles. The ambient wind direction is indicated by the big arrow at the top left corner of the figure. The unsteady forcing in this model (varying ambient wind speed) changes the shape and location of the portal vortex but does not threaten its existence.

and  $t$  variables). We visualize this slow manifold by first taking a  $z(t)=z_p(t)$  slice of  $M_\epsilon$ —where  $z_p(t)$  is the time-varying vertical coordinate of an inertial particle, then plotting the resulting two-dimensional time-varying surface in the  $(x, y, |\mathbf{v}|)$  coordinate space.

Figure 2 shows the projection of such a two-dimensional

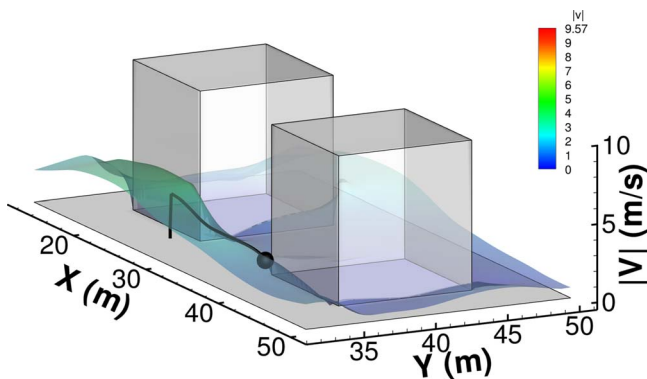


FIG. 2. (Color online) Projection of the two-dimensional  $z=z_p(t)$  slice of the slow manifold to the  $(x, y, |\mathbf{v}|)$  coordinate space. [Here  $z_p(t)$  is the time-varying  $z$ -coordinate of an inertial particle released near an upwind building.] The black solid line inside the street canyon indicates the particle's horizontal location and its velocity norm. Note the quick acceleration and convergence of the particle toward the slow manifold.

slice of the slow manifold at  $z_p=0.7525$  m, 6 s after the release of a finite-size particle at rest. The color scale indicates the magnitude of the slow manifold velocity  $|\mathbf{v}|$  at height  $z_p$ ; the largest value is between the two upwind buildings in the streamwise canyon (only one of the upwind buildings is shown). The black solid line shows the evolution of the horizontal location  $(x, y)$ , as well as the velocity norm  $|\mathbf{v}|$  of the finite-size particle we are following, where the particle velocity is the solution of Eq. (1). After the initial release of the particle with zero velocity, it accelerates quickly (hence the vertical “shoot-up” of the particle velocity) to synchronize with the slow manifold velocity. Subsequently, the particle stays close to the slow manifold.

In Fig. 3, we study particle dispersion and inversion using the full Maxey–Riley Eqs. (1). A set of 9702 finite-size particles representing anthrax spores are initially released at the Southeast edge of an upwind building at rest. This emulates the case of free release of a toxin by humans in urban streets. We use a fractional-step, semi-implicit numerical scheme to integrate Eq. (1) for particle trajectories. Particle velocities are solved for on fractional time step using a three-stage, fourth-order Lobatto IIIA method,<sup>22</sup> particle positions are solved for using the regular fourth-order explicit Runge–Kutta method. The time stepping for forward-time trajectories is 0.005 s and that for the backward-time trajectories is

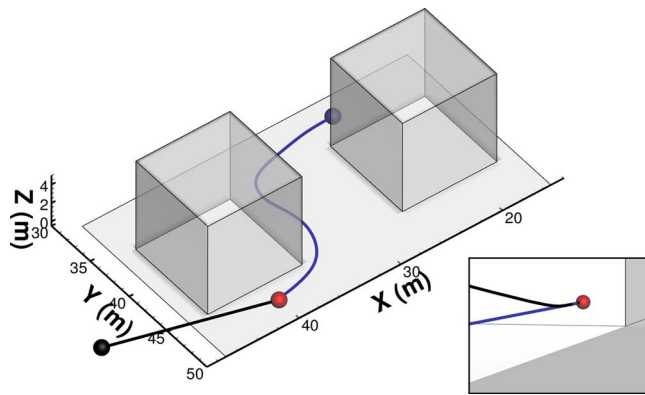


FIG. 3. (Color online) Anthrax dispersion and its inversion using the full Maxey–Riley Eq. (1) for one of the ensemble of trajectories. The blue sphere indicates the original release location of the particle near the upwind building. The blue solid line indicates the forward-time dispersion of this particle and the red sphere shows its end position 20 s after release. Direct backward integration of Eq. (1) (black solid line and sphere) indicates a quick numerical blowup of the trajectory in backward time. The inset shows this blowup even at the very beginning of the source inversion.

0.001 s. This ensures better numerical stability in the evolution of particle velocity. A typical particle trajectory is chosen for Fig. 3 to demonstrate the quick blowup when solving for Eq. (1) in backward time.

The release location of the particle is indicated by the blue sphere. The forward-time particle trajectory in the next 20 s (the blue line) shows that this particle is entrained into the horseshoe vortex and traverses the spanwise canyon. Its end location is marked by a red sphere. Directly integrating Eq. (1) in backward time leads to numerical instability in the vicinity of the start of the inversion (the black trajectory and sphere showing that the inverted particle is erroneously leaving the domain). The inset shows an enlarged vision of the blowup, very shortly after the start of the inversion. The blowup occurs because we are practically integrating an equation of the type  $\dot{v} = -v/\epsilon$  in backward time with  $\epsilon \ll 1$ . Numerical error quickly accumulates even though a highly accurate implicit scheme is used to solve this equation. In Fig. 4, we randomly choose five trajectories in different flow regions, and integrate them in backward time using Eq. (1).

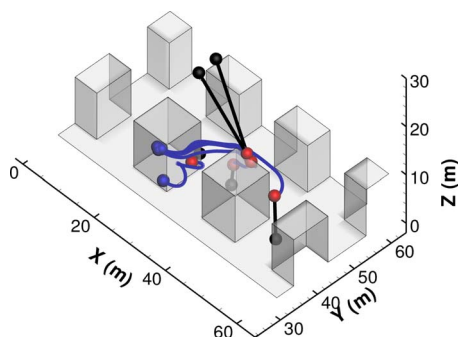


FIG. 4. (Color online) Five random trajectories chosen from different regions of the flow. Their inversion using Eq. (1) shows that numerical blowup is inevitable for the inversion procedure used. The color schemes are the same as in Fig. 3.

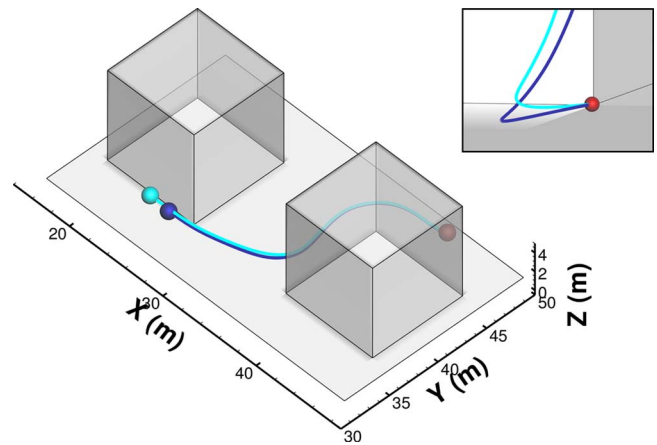


FIG. 5. (Color online) Source inversion using  $\dot{\mathbf{x}} = \mathbf{u}(\mathbf{x}, t)$ . The cyan solid line indicates a backward-time particle trajectory for  $\epsilon = 0$ , i.e., the trajectory of an infinitesimal fluid particle. This trajectory does not blow up but is inaccurate. The inset shows its deviation from the true particle trajectory (blue solid line) from the start of the inversion.

The result shows that even with the higher-order numerical method we use, the numerical blowup of backward-time trajectories is inevitable.

Motivated by the smallness of the parameter  $\epsilon$ , we have also considered the inversion using the ambient flow velocity  $\mathbf{u}$ . This idealized inversion process neglects all inertial effects in locating the source of the contamination. The results are shown in Fig. 5. The cyan solid line and sphere show the backward-time trajectory and the final position obtained from the idealized source inversion procedure. Clearly, by comparison with the forward-time trajectory and the true source, this procedure leads to a bounded yet inaccurate result.

Even though  $\mathbf{u}$  only differs by an  $\mathcal{O}(\epsilon)$  term from the right-hand side of the inertial Eq. (3), the backward trajectories of the two velocity fields can be very different. This is because Eq. (3) on the slow manifold has sensitive dependence on initial conditions; as a result, even an  $\mathcal{O}(\epsilon)$  perturbation to it can lead to dramatically different trajectories over appropriately long time scales.

Finally, we demonstrate the source inversion technique proposed by Haller and Sapsis.<sup>7</sup> We solve Eq. (3) in backward time using a fourth-order explicit Runge–Kutta method with the results shown in Fig. 6. Inversion trajectory and inverted source location are marked by the green line and green sphere. As seen in the figure, the backward-time particle trajectory obtained from the inertial Eq. (3) is indistinguishable from the forward-time particle trajectory except in the vicinity of the source (cf. the inset).

In Fig. 7, we show the advantage of using the slow manifold approach in source inversion for an ensemble of 9702 particles released at 1.5 and 8 m from rest near the Southeast corner of the upwind building. The end locations of these particles 20 s after release are shown as red sphere that outline the main flow features.

We compare the results of source inversion for the two numerically stable approaches. On the left of Fig. 7, source inversion is carried out using fluid velocity. Inverted

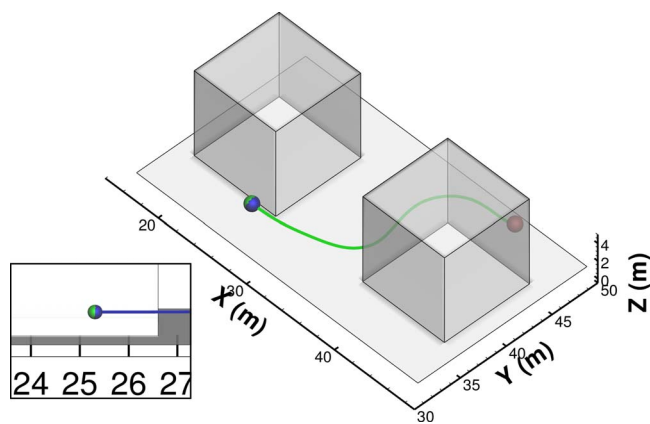


FIG. 6. (Color online) Source inversion on the slow manifold using Eq. (3). The green line is the backward-time particle trajectory; its end position marked by the green sphere. Note that the inertial particle ends up close to its source when solved for using Eq. (3). The inset shows an enlarged view at the end of the inversion.

“sources” are shown as cyan spheres. The result shows substantial deviation from the true sources.

On the right of Fig. 7, we use the inertial Eq. (3) to advect particles in backward time. The inverted sources are marked by green spheres. Note that almost all particles return closely to their origin. The handful of inaccurate trajectories are due to numerical errors coupled with sensitive dependence on initial conditions in the chaotic flow generated by Eq. (3).

It is worth noting that most trajectories on the right of Fig. 7 return to the same small volume, pinpointing that the Southeast edge of the upwind building was the site of the outbreak. Therefore, using the inertial equation enables us to locate the contamination source without knowing explicitly the time of release.

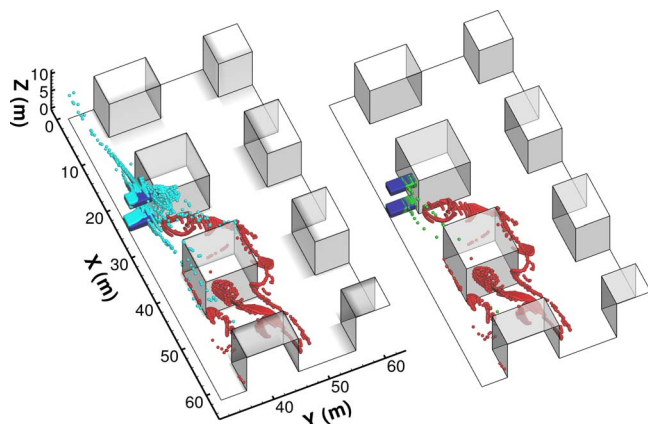


FIG. 7. (Color online) Source inversion using fluid velocity and slow manifold velocity for two clusters of particle clouds (total of 9702 particles). The clusters start at the Southeast edge of an upwind building, as blue cubic blobs. Particle positions 20 s after release are shown as red spheres. Inversion by fluid velocity (cyan spheres) show significant inaccuracies due to trajectories entering different flow topologies. Inversion by slow manifold velocity (green spheres) shows excellent accuracy with only very few exceptions. The latter are due to numerical inaccuracies in solving the flow on the slow manifold in backward time.

As proved in Haller and Sapsis,<sup>7</sup> the difference of inverted particle positions near the source is  $\mathcal{O}(\epsilon)$  small, i.e., of the order of centimeters in our present example. Since there is no numerical instability on the slow manifold, a much larger time step is sufficient when we compute backward-time particle trajectories. This enables fast response to an event of pollutant outbreak.

## VIII. DISCUSSIONS AND CONCLUSIONS

In summary, an exponential instability in the backward-time Maxey–Riley equations makes it practically impossible to find the release location of contamination by small particles. By contrast, projection onto, and subsequent backward integration along, the slow manifold renders the release location with high accuracy.

In a practical implementation, the manifold-based source inversion procedure used here works on time scales where diffusion can be neglected relative to advection, and time-resolved wind data are available in the spatial region of interest. Such wind data may be obtained from ground-based LIDAR scans or from numerical simulation fitted to sensor observations.

Our numerical experiments showed that the slow-manifold-based source inversion scheme proposed by Haller and Sapsis<sup>7</sup> accurately recovers the initial position of a set of nondiffusive particles even under fairly complex geometries. Only a handful of particles (out of thousands) go astray in the inversion procedure due to numerical inaccuracies in their advection. Such a small leakage is inevitable in inverting a complex flow numerically; its extent can be reduced by choosing a more accurate backward numerical advection scheme on the slow manifold.

An interesting question is the maximal value of  $\epsilon = St/R$  below which the inversion procedure employed here is valid. A limitation on the admissible  $\epsilon$  in a particular flow field is given by inequality Eq. (5). When this inequality fails, the slow manifold develops local instabilities, but it may still keep acting as a global attractor for particles, validating our inversion procedure. We expect the latter to be the case for moderately turbulent flows. The inversion procedure is certain to fail if the slow manifold suffers a global loss of stability, i.e., Eq. (5) fails to be satisfied on most of the flow domain of interest. Such a global instability requires large velocity gradients typical in severely turbulent flows.

In our experience, a global loss of stability for the slow manifold is preceded by the breakdown of the Maxey–Riley equations as a reasonable approximation for inertial particle motion. For higher particle Reynolds numbers that are still below  $Re_p = 1000$ , we may use the Basset–Boussinesq–Oseen (BBO) equations instead of the Maxey–Riley equations (Crowe *et al.*).<sup>23</sup> The structure of the BBO equations is similar to the Maxey–Riley equations, while some of the parameters in the BBO equations are fitted to match experiments. Because of the structural similarities (notably, the presence of two time scales in the particle dynamics), the slow manifold and the associated source inversion approach described here remain applicable to the BBO equations, provided that the slow manifold remains globally attracting.

## ACKNOWLEDGMENTS

This work was supported by the Air Force Office of Scientific Research under Grant No FA9550-06-1-0101. We are grateful to Themis Sapsis for helpful discussions. We also thank two anonymous referees for their valuable critiques and comments.

- <sup>1</sup>M. R. Maxey and J. J. Riley, "Equation of motion for a small rigid sphere in a nonuniform flow," *Phys. Fluids* **26**, 883 (1983).
- <sup>2</sup>T. R. Auton, J. C. R. Hunt, and M. Prud'Homme, "The force exerted on a body in inviscid unsteady non-uniform rotational flow," *J. Fluid Mech.* **197**, 241 (1988).
- <sup>3</sup>A. Babiano, J. H. E. Cartwright, O. Piro, and A. Provenzale, "Dynamics of a small neutrally buoyant sphere in a fluid and targeting in Hamiltonian systems," *Phys. Rev. Lett.* **84**, 5764 (2000).
- <sup>4</sup>I. J. Benczik, Z. Toroczkai, and T. Tél, "Selective sensitivity of open chaotic flows on inertial tracer advection: Catching particles with a stick," *Phys. Rev. Lett.* **89**, 164501 (2002).
- <sup>5</sup>M. R. Maxey, "The motion of small spherical particles in a cellular flow field," *Phys. Fluids* **30**, 1915 (1987).
- <sup>6</sup>L. P. Wang, M. R. Maxey, T. D. Burton, and D. E. Stock, "Chaotic dynamics of particle dispersion in fluids," *Phys. Fluids A* **4**, 1789 (1992).
- <sup>7</sup>G. Haller and T. Sapsis, "Where do inertial particles go in fluid flows," *Physica D* **237**, 573 (2008).
- <sup>8</sup>J.-F. Sini, S. Anquetin, and P. G. Mestayer, "Pollutant dispersion and thermal effects in urban street canyons," *Atmos. Environ.* **30**, 2659 (1996).
- <sup>9</sup>J.-J. Kim and J.-J. Baik, "A numerical study of the effects of ambient wind direction on flow and dispersion in urban street canyons using the RNG  $k-\varepsilon$  turbulence model," *Atmos. Environ.* **38**, 3039 (2004).
- <sup>10</sup>E. Mograbi and E. Bar-ziv, "On the asymptotic solution of the Maxey-Riley equation," *Phys. Fluids* **18**, 051704 (2006).
- <sup>11</sup>J. Rubin, C. K. R. T. Jones, and M. Maxey, "Settling and asymptotic motion of aerosol particles in a cellular flow field," *J. Nonlinear Sci.* **5**, 337 (1995).
- <sup>12</sup>T. J. Burns, R. W. Davis, and E. F. Moore, "A perturbation study of particle dynamics in a plane wake flow," *J. Fluid Mech.* **384**, 1 (1999).
- <sup>13</sup>S. L. Rani and S. Balachandar, "Evaluation of the equilibrium Eulerian approach for the evolution of particle concentration in isotropic turbulence," *Int. J. Multiphase Flow* **29**, 1793 (2003).
- <sup>14</sup>O. A. Druzhinin, "On the two-way interaction in two-dimensional particle-laden flows: The accumulation of particles and flow modification," *J. Fluid Mech.* **297**, 49 (1995).
- <sup>15</sup>J. Ferry and S. Balachandar, "A fast Eulerian method for disperse two-phase flow," *Int. J. Multiphase Flow* **27**, 1199 (2001).
- <sup>16</sup>E. Balkovsky, G. Falkovich, and A. Fouxon, "Intermittent distribution of inertial particles in turbulent flows," *Phys. Rev. Lett.* **86**, 2790 (2001).
- <sup>17</sup>T. Sapsis and G. Haller, "Instabilities in the dynamics of neutrally buoyant particles," *Phys. Fluids* **20**, 017102 (2008).
- <sup>18</sup>G. Haller, "Distinguished material surfaces and coherent structures in 3D fluid flows," *Physica D* **149**, 248 (2001).
- <sup>19</sup>M. Mathur, G. Haller, T. Peacock, J. E. Ruppert-Felsot, and H. L. Swinney, "Uncovering the Lagrangian skeleton of turbulence," *Phys. Rev. Lett.* **98**, 144502 (2007).
- <sup>20</sup>S. C. Shadden, F. Lekien, and J. E. Marsden, "Definition and properties of Lagrangian coherent structures from finite-time Lyapunov exponents in two-dimensional aperiodic flows," *Physica D* **212**, 271 (2005).
- <sup>21</sup>F. Lekien, S. C. Shadden, and J. E. Marsden, "Lagrangian coherent structures in  $n$ -dimensional systems," *J. Math. Phys.* **48**, 065404 (2007).
- <sup>22</sup>E. Hairer, C. Lubich, and G. Wanner, *Geometric Numerical Integration: Structure-Preserving Algorithms for Ordinary Differential Equations*, 2nd ed. (Springer-Verlag, Berlin, 2006).
- <sup>23</sup>C. Crowe, M. Sommerfeld, and Y. Tsuji, *Multiphase Flows with Droplets and Particles* (CRC, Boca Raton, FL, 1998).